which should be cited to refer to this work.

Intrinsic Distortion Path in the Analysis of the Jahn-Teller Effect

Matija Zlatar[a,b], Maja Gruden-Pavlović[a,c], Carl-Wilhelm Schläpfer[a], Claude Daul[*,a]

[a] *Department of Chemistry, University of Fribourg, Fribourg, Switzerland*
[b] *Center for Chemistry, IHTM, University of Belgrade, Belgrade, Serbia*
[c] *Faculty of Chemistry, University of Belgrade, Belgrade, Serbia*

Abstract

The multideterminental-DFT approach was performed in order to calculate the Jahn-Teller (JT) parameters for the JT active molecules. Within the harmonic approximation the JT distortion can be analysed as a linear combination of all totally symmetric normal modes in any of the low symmetry minimum energy conformation, which allows to calculate the Intrinsic Distortion Path (IDP), exactly from the high symmetry point to the low symmetry configuration. Results obtained by both methods are consistent and give direct insight into the coupling of electronic structure and nuclear movements. As examples, the results for Cu_3 cluster, cobaltocene and manganocene are reported.

Key words: Intrinsic Distortion Path, Jahn-Teller Effect, Density Functional Theory, Cu_3, Metallocenes

1. Introduction

Even though it passed over 70 years from the publication of the seminal paper of Jahn and Teller [1], the effect named after its authors continues to be a subject of interest in various fields of chemistry and physics. The theory underlying the Jahn-Teller (JT) and related effects, is well known and

[*]Corresponding author
Email addresses: matija.zlatar@unifr.ch (Matija Zlatar), claude.daul@unifr.ch (Claude Daul)

documented in detail [2]. In this paper we are presenting a new approach to the detailed interpretation of the latter one based on Density Functional Theory (DFT) calculations, which was recently proposed [3].

The molecule with a degenerate electronic state prone to a JT distortion has a nuclear arrangement that belongs to a high symmetry (HS) point group. As a consequence of the degenerate electronic state this arrangement is not a stationary point on the potential energy surface. The molecule distorts along non-totally symmetric vibrational coordinates. This leads to an energy minimum on the potential energy surface, which corresponds to a nuclear arrangement of lower symmetry (LS). This distortion is expressed in various molecular properties, i.e. geometry, spectroscopic, magnetic properties etc. [2]. Quantifying the distortion and stabilization energy and getting insight into the mechanism is of great interest and goes beyond the interpretation of the molecular spectra, and the prediction of the minimum energy conformation. At the HS point, Born-Oppenheimer (BO), or adiabatic approximation breaks down. There is a vibronic coupling between the electron distribution and a displacements of the nuclei. It needs to be pointed out that traditional computational methods can still be used even where non-adiabatic effects are important, if a perturbation approach is introduced to the BO approximation. This is possible if the adiabatic potential energy surface can be accurately determined, as it is case with the DFT.

The vibronic coupling is of the crucial importance in chemistry. Each chemical reaction starts with a perturbation of the electron distribution, which induces a movement of the nuclei leading to the reaction. Our interpretation of the JT distortion allows a direct insight into the coupling and contributes thereby to the understanding of the reaction pathways. In this sense there is a close resemblance between the JT distortion and reaction paths, which was often overlooked. This analogy can be understood if one compares energy profiles along the typical reaction and JT distortion (Fig. 1).

The transition state (TS) of a reaction corresponds to a energy maximum along the reaction coordinate and there will be a coupling between electron density and movements of nuclei. A movement along the reaction coordinate, $Q_a(\mathrm{RC})$, on the potential energy surface leads to the stabilization of the system by the destruction of the pseudomolecule and rearrangement of the nuclei into either reactants (R) or products (P). The chemical reaction is characterized with a set of parameters with a clear physical meaning: the activation energy (E_a), the reaction energy (E_r) and the reaction path ($Q_a(\mathrm{RC})$), Fig.

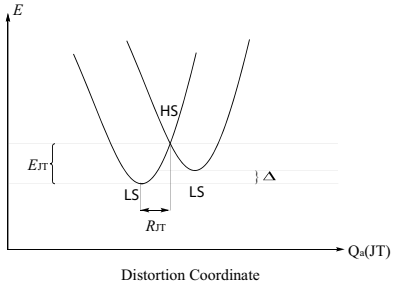

(a) Indication of the JT parameters: the JT stabilisation energy, E_{JT}, the warping barrier, Δ, the JT radius, R_{JT}

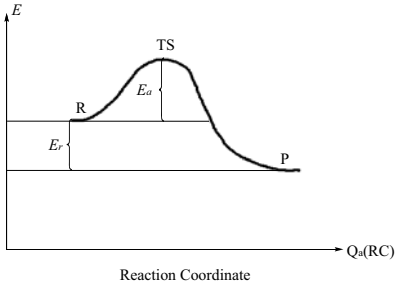

(b) Energy Profile along the typical chemical reaction: activation energy, E_a, reaction energy, E_r

Figure 1: Analogy between the JT distortion and the chemical reaction path: Qualitative cross section through the adiabatic potential energy surface, along JT coordinate Q_a(JT), (a), and reaction coordinate Q_a(RC), (b)

1(b). Similarly the HS structure of the JT system corresponds to a cusp on the adiabatic potential energy surface. Vibronic coupling suppresses the crossing of the energy surfaces predicted in the BO approximation. By analogy the JT distortion can be described with: the JT stabilisation energy (E_{JT}), the warping barrier (Δ) and the distortion path (Q_a(JT)), Fig. 1(a). The goal of the analysis of JT systems is the determination of these parameters. To achieve this it is necessary either to perform an experiment, and fit the results to the proposed model, or today to carry out a computational study. Our group is doing ongoing research in the latter by the means of the DFT.

Recently, we have extended the analysis of the JT distortion as a superposition of normal coordinates [3]. Our model is based on the theory of chemical reactions of Bader [4, 5, 6], Pearson [7, 8] and Fukui [9, 10]. The JT distortion represents a linear displacement from the HS conformation to the LS energy minimum on the $3N-6$ dimensional potential energy surface. It corresponds to a linear combination of displacements along all the totally symmetric normal coordinates of the energy minimum structure. Topologically it is given by the projection of the normal coordinates on the JT distortion. The method we proposed [3] allows the separation of their contributions in the direct way. This is in contrast to the usual treatment of the JT effect, which starts from the HS configuration. Our approach to the

multimode JT problem is alternative to the method based on the coordinate transformation, as described in [2] and applied recently by Liu et al. [11].

Within the harmonic approximation the potential energy surface has a simple analytical form which allows to calculate the path of minimal energy, Intrinsic Distortion Path (IDP), step by step from the HS point to the LS energy minimum. Analysis of this path is of interest, because it gives direct insight into the coupling of electronic structure and nuclear movements. The IDP analysis answers the questions, which are the totally symmetric normal coordinates of the LS structure that contribute to the JT distortion at the HS point and how does their contribution change along the IDP.

2. Methodology

2.1. Density Functional Calculations

The DFT calculations reported in this work have been carried out using the Amsterdam Density Functional program package, ADF2007.01 [12, 13, 14]. The local density approximation (LDA) characterized by the Vosko-Willk-Nusair (VWN) [15] parameterization have been used for the geometry optimizations. Triple zeta (TZP) Slater-type orbital (STO) basis set have been used for all atoms. All calculations were spin-unrestricted and for numerical integration ten significant digits are used. The analytical harmonic frequencies were calculated [16, 17], and analysed with the aid of PyVib2 1.1 [18].

2.2. Calculation of the Jahn-Teller Stabilization Energy

The method for calculation of the JT parameters using DFT was developed in our group [19]. The detailed explanation of computational recipe was recently reviewed [3]. Briefly, it is necessary to know geometries and energies of the HS and the LS points to get the JT parameters. For the LS structure, as the system is in a non-degenerate electronic ground state, this is straightforward. Electronic structure of the HS point, on the other hand, must be represented with at least two Slater determinants, consequently, using a single determinant DFT is troublesome. A method based on the multideterminental-DFT, is therefore used. In order to get the geometry of the HS point, we use the average of configuration geometry optimization with fractional orbital occupation. To obtain the energies of the degenerate states at the HS one needs to evaluate the energies of all possible single determinants with integer occupations in the HS geometry. This is achieved by

introducing an adequate occupation scheme of the Molecular Orbitals (MOs). E_{JT} is the difference between the energies of the degenerate state of HS and the non-degenerate of LS.

Table 1: Results of multideterminental-DFT calculations performed to analyse the JT effect of selected compounds; energies are given in $10^3\mathrm{cm}^{-1}$; N is the number of atoms in a molecule; N_{a_1} is the number of totally symmetrical vibrations in LS minimum

	Distortion	E_{JT}(DFT)	E_{JT}(exp)	$3N-6$	N_{a_1}
Cu_3	$D_{3h} \longrightarrow C_{2v}$	**0.53** [1]	0.28-0.55 [2]	3	2
VCl_4	$T_d \longrightarrow D_{2d}$	**0.04** [19]	0.03-0.08[20, 21, 22, 23]	9	2
$C_5H_5^{\cdot}$	$D_{5h} \longrightarrow C_{2v}$	**1.25** [3]	1.24 [24]	24	9
$CoCp_2$	$D_{5h} \longrightarrow C_{2v}$	**0.81** [25]	0.15-1.05 [26]	57	16
$MnCp_2$	$D_{5h} \longrightarrow C_{2v}$	**0.71** [1]	~ 0.35 [26, 27]	57	16
$Cu(en)_3^{2+}$	$D_3 \longrightarrow C_2$	**2.12** [28]	2.00 ± 0.20 [29]	105	53

[1] This work

The results demonstrate that this DFT procedure allows to predict the E_{JT} for different systems with a reasonable accuracy (Table 1). This is of interest because the experimental determination of the JT parameters is often difficult, and there is an uncertainty in the values.

2.3. Intrinsic Distortion Path

Following the equation of Fukui [9, 10], Intrinsic Distortion Path (IDP), $\vec{R}_{\mathrm{IDP}}(t)$ is given as a solution of the following first order Ordinary Differential Equation:

$$\frac{d\vec{R}(t)}{dt} = -\frac{dV(t)}{dt} \tag{1}$$

where $0 \leq t < \infty$. If the potential is harmonic, $V(t) = \frac{1}{2}\vec{R}(t)^T \mathbb{H} \vec{R}(t)$, this equation reads:

$$\frac{d\vec{R}(t)}{dt} = -\mathbb{H}\vec{R}(t) \tag{2}$$

It is easy to show that the solution of the eq. (2) is:

$$\vec{R}_{\mathrm{IDP}}(t) = \mathbb{U}\mathrm{diag}[exp(-\lambda_i t)]\mathbb{U}^T \vec{R}(t=0) \tag{3}$$

with diag$[\lambda_i] = \mathbb{U}^T\mathbb{H}\mathbb{U}$, $\mathbb{H}$ is the Hessian, $\lambda_{\rm i}$ and the i-th column of the matrix $\mathbb{U}$ are respecively the i-th eigenvalue and the corresponding eigenvector of the $\mathbb{H}$ at the LS minimum energy configuration. $\vec{R}(t=0) = \vec{R}_{\rm HS}$ are coordinates of the HS configuration. Geometry of LS energy minimum is chosen to be the origin of the configuratin space, $\vec{R}(t=\infty) = \vec{R}_{\rm LS} = \vec{0}$. Every point $\vec{X}$ on the potential energy surface can be represented by a $3N$ dimensional vector $\vec{R}_{\rm X}$, using mass-weighted generalized coordinates relative to the origin. The potential energy surface within harmonic approximation is defined as a superposition of $N_{a_1} \leq 3N-6$ totally symmetric orthogonal oscillators in LS. As a consequence any displacement in the configuration space is given by a superposition of displacements along the totally symmetric normal coordinates. Thus, within the harmonic approximation it is possible to express $\vec{R}_{\rm X}$ as a linear combination of N_{a_1} totally symmetric normal coordinates in LS:

$$\vec{R}_{\rm X}(t) = \mathbb{Q}\vec{w}_{\rm X}(t) \tag{4}$$

where $\vec{w}_{\rm X}$ is the N_{a_1} dimensional vector containing the weighting factors, $w_{\rm Xk}$ which represent the contribution of the displacements along the different totally symmetric normal coordinates to the $\vec{R}_{\rm X}$; $\mathbb{Q}$ is the $3N \times N_{a_1}$ matrix with the columns being the $\vec{Q}_{\rm k}$, totally symmetric normal coordinates which are the eigenvectors of the Hessian, obtained by the DFT frequency calculations in the LS minimum energy conformation. The corresponding eigenvalues are $\lambda_{\rm k} = (2\pi\nu_{\rm k})^2$, $\nu_{\rm k}$ is a frequency of the k-th normal mode. Equation (4) can be solved to get the weighting factors $w_{\rm Xk}$:

$$\vec{w}_{\rm X} = (\mathbb{Q}^T\mathbb{Q})^{-1}\mathbb{Q}^T\vec{R}_{\rm X} \tag{5}$$

The energy of the nuclear configuration $\vec{R}_{\rm X}$, $E_{\rm X}$, relative to the LS energy minimum $E_{\rm LS}$ is expressed as the sum of the energy contributions of the N_{a_1} totally symmetric normal modes:

$$E_{\rm X} = \sum_{\rm k=1}^{N_{a_1}} E_{\rm k} = \frac{1}{2}\sum_{\rm k=1}^{N_{a_1}} w_{\rm Xk}^2 \vec{Q}_{\rm k}^2 \lambda_{\rm k} \tag{6}$$

The force $\vec{F}_{\rm Xk}$ driving the system to the LS energy minimum (origin) at any point $\vec{R}_{\rm X}$ is defined as a derivative of the energy over the Cartesian coordinates. The total distortion force is given as a vector sum of the individual forces. In the HS point indicates the driving force for the JT distortion.

$$\vec{F}_{\mathrm{Xtot}} = \sum_{\mathrm{k}=1}^{N_{a_1}} \vec{F}_{\mathrm{Xk}} = \sum_{\mathrm{k}=1}^{N_{a_1}} w_{\mathrm{Xk}} \lambda_{\mathrm{k}} \mathbb{M}^{1/2} \vec{Q}_{\mathrm{k}} \tag{7}$$

where $\mathbb{M}$ is a diagonal $3N \times 3N$ matrix with atomic masses in triplicates as elements (m_1, m_1, m_1, m_2, ..., m_N). $\vec{F}_{\mathrm{Xtot}}$, the force which drives the nuclei to the LS minimum gives the direction from one to the another point on the adiabatic potential energy surface in a way of maximizing decrease of the energy. Path from the HS to the LS minimum obtained in this way is the Intrinsic Distortion Path (IDP). The vector $\vec{R}_{\mathrm{HS}} = \vec{R}_{\mathrm{JT}}$ defines the straight path (Direct Path) from the HS configuration to the LS energy minimum configuration. This is in general different from the IDP.

In principal the Intrinsic Reaction Coordinate (IRC) method [9, 10] implemented in conventional quantum chemistry program packages, can be used for the calculation of the IDP. Unfortunately the first step along the IRC gives already about 2/3 of the JT stabilisation energy [3]. This is due to the fact that IRC algorithm implemented locates the minimum in the fastest way. Thus, the information from the first small step breaking the high symmetry is missing. With our model it is possible to quantify the contribution of all normal modes, their energy contribution to the E_{JT}, the forces at the HS point and the detailed distortion path. Matlab scripts for these calculations can be obtained from authors upon request.

3. Results and Discussion

All molecules mentioned in the Table 1 have a doubly degenerate electronic ground state, which is coupled with vibrations of a doubly degenerate irreducible representation in the HS point group. They belong to $E \otimes e$ JT systems. The systems differ in the nature of chemical bonding, symmetry of the distortion, range of E_{JT} and the number of atoms, hence the number of different normal modes that need to be considered.

Group theory allows finding the irreducible representation of the non-totally symmetric vibrations in the HS conformation, which are JT active, remove the degeneracy and lead to a stabilization of the system by lowering the symmetry. The irreducible representations of the active modes, $\Gamma_{\mathrm{HS}}^{vib}$ are given by the direct product $\Gamma_{\mathrm{HS}}^{elect} \otimes \Gamma_{\mathrm{HS}}^{elect} \subset A_1 + \Gamma_{\mathrm{HS}}^{vib}$ in HS point group. The point group of the LS minimum energy conformation is defined by the requirement that the irreps of the active modes become totally symmetric upon

descent in symmetry and the application of the epikernal principle [2, 30, 31]. In the LS point group these modes might mix with a_1 vibrations which are always present in the direct product and never change upon descent in symmetry. In many situations other irreps in HS, which are not contained in the direct product, may become totally symmetric upon descent in symmetry and therefore contribute also to the JT distortion. This is found in the case of the JT $D_{5h} \rightarrow C_{2v}$ distortion [3], e.g. for $C_5H_5^{\cdot}$ radical, cobaltocene and manganocene, where the normal coordinates that are basis of the e_2', e_1' and a_1' irreducible representations in D_{5h} become a_1 in C_{2v}.

Hence, at least two normal coordinates need to be considered in the detailed analysis of the JT problems. The results for a Cu_3 cluster, with only two, and metallocenes (cobaltocene and manganocene), with 16 totally symmetric normal modes in LS, are presented in order to illustrate the concepts of the IDP method. It is noteworthy that results obtained by the IDP method performed on all the molecules in Table 1, are in a good agreement with ones obtained by multideterminental-DFT procedure. This holds even in a case of $[Cu(en)_3]^{2+}$ when we deal with 53 totally symmetric normal modes.

3.1. Cu_3 Cluster

The trimer Cu_3 is one of the simplest molecules that exhibit Jahn-Teller effect. It has a $^2E'$ electronic ground state in regular triangular nuclear configuration, D_{3h} point group. Using group theory it can be shown that distortion coordinate is e' ($E' \otimes E' \subset A_1' + [A_2'] + E'$) and distortion goes to C_{2v}. The electronic state will split into A_1 and B_2, while the degenerate JT active distortion e' splits into a_1 and b_2. Only one component of the degenerate vibration is JT active. It should be pointed out that a_1' normal coordinate in D_{3h} in addition to the a_1' component of e' has a non zero gradient, although not lowering the symmetry.

DFT calculations, Table 2, show that minima on the potential energy surface corresponds to obtuse triangle geometry ($^2B_2$) while transition states to acute ($^2A_1$), which is consistent with the previous studies on this system [2]. E_{JT} obtained by multideterminental-DFT (525 cm^{-1}) and with the IDP method (370 cm^{-1}) fall in the range of the values obtained till now (Table 1.) [2]. Different values obtained by the two methods are probably due to the anharmonicity of this system [32]. Since the IDP model is based on a harmonic approximation, it is not surprising to obtain smaller stabilization energy. Still, the IDP results provide a good basis for the discussion of the distortion. The JT distortion and the JT stabilisation arise mainly from the

Table 2: Results of the DFT calculations performed to analyse the JT effect of Cu_3; energies (LDA) are given in eV; the JT parameters E_{JT} and Δ are given in cm^{-1} and R_{JT} in $(\mathrm{amu})^{1/2}$Å

Occupation	State	Geometry	Energy
$e'^{0.5}e'^{0.5}$	$^2E'$	D_{3h}	-4.8702
$b_2^1a_1^0$	$^2B_2$	D_{3h}	-4.8290
$a_1^1b_2^0$	$^2A_1$	D_{3h}	-4.8224
$b_2^1a_1^0$	$^2B_2$	C_{2v}	-4.8942
$a_1^1b_2^0$	$^2A_1$	C_{2v}	-4.8798
E_{JT}	$^2B_2$		525
E_{JT}	$^2A_1$		463
Δ			116
R_{JT}	$^2B_2$		1.12
R_{JT}	$^2A_1$		0.82

e' type vibration (Vib. 1). It contributes 97 % to the distortion $\vec{R}_{\mathrm{JT}}$, and 88 % to the E_{JT}. Still, it would be erroneous not to consider the a_1' type Vib.2 (breathing). Figure 2 (a) shows the difference between the Direct Path, where the contributions of two totally symmetric modes are constant, and the IDP. The contributions of the two modes along the path are changing, Fig. 2 (b) and Fig. 3. In the first step Vib. 2 contributes ca. 35% to the IDP and fades out in the late steps.

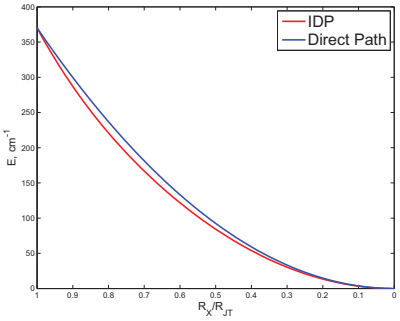

(a) Difference between the Direct Path and IDP

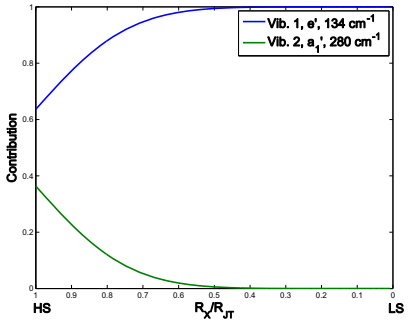

(b) Changes of contributions (normalized to 1) of the two normal modes to the distortion along IDP in Cu_3

Figure 2: Results of the IDP method for the JT distortion in Cu_3

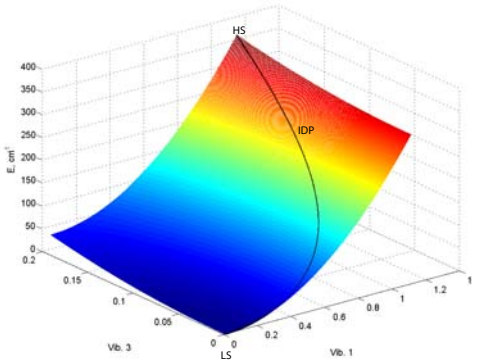

Figure 3: 3D representation of the adiabatic potential energy surface (E in cm^{-1}) along the two a_1 vibrations of Cu_3 in C_{2v}, Vib. 1 and Vib. 3 (in Å); indication of the IDP

In Fig. 4 vibrational energy distribution representation [33] of this two a_1 vibrations in C_{2v} symmetry is presented. Different colours indicate the direction of the displacement vector, and a volume of the spheres is proportional to the contribution made by individual nuclei to the energy of the vibrational mode. In order to be consistent with usual treatments of the JT effect, correlation of the vibrations [33] in C_{2v} and in D_{3h} point groups is also illustrated, Fig. 5. A circle with a diameter equal to the square which contains it means a value of 1.

(a) Vib.1 corresponding to e'_1, 134 cm^{-1}

(b) Vib.3 corresponding to a'_1, 280 cm^{-1}

Figure 4: Vibrational energy distribution representation of Vib.1, (a) and of Vib.3, (b), in Cu_3

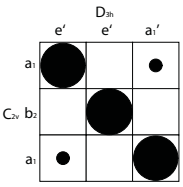

Figure 5: Correlation between the vibrations in D_{3h} and C_{2v} conformations of Cu_3

3.2. Cobaltocene vs Manganocene

The high symmetry conformation of metallocenes is either D_{5h} if the two rings are eclipsed or D_{5d} if the two rings are staggered. According to the DFT calculations eclipsed conformation is more stable one [25, 34, 35]. Our recent study showed that the internal rotation of the rings does not influence the JT distortion [25]. The energy barrier upon rotation is much smaller than the JT stabilization.

JT instable metallocenes, e.g d^7 cobaltocene ($CoCp_2$) and low-spin d^5 manganocene ($MnCp_2$), are typical examples of the multimode JT distortions. The descent in symmetry goes from D_{5h} to C_{2v} (taking the eclipsed conformations of the rings). Details about multideterminental DFT results of the JT effect in cobaltocene, as well as thorough group theoretical analysis of the $D_{5h} \rightarrow C_{2v}$ JT effect can be found in our previous papers [3, 25]. DFT results for manganocene are summarized in Table 3. For cobaltocene $E_{\mathrm{JT}}(\mathrm{DFT}) = 814$ cm^{-1}, and for manganocene $E_{\mathrm{JT}}(\mathrm{DFT}) = 708$ cm^{-1}, the warping barrier Δ is 0 for both cases, as predicted by group theory.

In C_{2v} minimum energy conformation, cobaltocene and manganocene have 16 totally symmetrical vibrations, which can all contribute to the distortion. Our approach to the multimode JT problem allows the determination of their contributions to the distortion and to the E_{JT} (Fig. 6, Table S1 in Supplementary Material), and a detailed description of the IDP.

The main contribution to the JT distortion in cobaltocene arises from the four e_2' type vibrations: the out-of-plane ring distortion, Vib. 4, the in-plane ring distortion, Vib. 7, the C−H wagging (the out-of-plane C−H bending), Vib. 8, and in-plane C−H bending, Vib. 10. The JT distortion in manganocene, on the other hand, arises from two e_1' type and one a_1' type vibrations. e_1's are: skeletal-bending, Vib. 1, and ring-tilt, Vib.3; a_1' is

Table 3: Results of the DFT calculations performed to analyse the JT effect of manganocene; energies (LDA) are given in eV; the JT parameters E_{JT} and Δ are given in cm^{-1} and R_{JT} in $(\mathrm{amu})^{1/2}$Å

Occupation	State	Geometry	Energy
$e_2'^{1.5}e_2'^{1.5}$	$^2E_2'$	D_{5h}	-143.7308
$b_2^2a_1^1$	$^2A_1$	D_{5h}	-143.6947
$a_2^1b_2^1$	$^2B_2$	D_{5h}	-143.6947
$b_2^2a_1^1$	$^2A_1$	C_{2v}	-143.7825
$a_2^1b_2^1$	$^2B_2$	C_{2v}	-143.7825
E_{JT}	$^2A_1$		708
E_{JT}	$^2B_1$		708
Δ			0
R_{JT}	$^2A_1$		0.77
R_{JT}	$^2B_1$		0.77

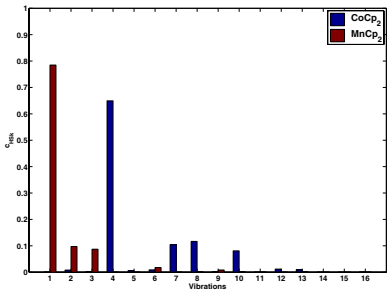

(a) Contribution of the 16 a_1 normal modes in C_{2v} (LS) to the total JT **distortion** in blue $CoCp_2$ and in red $MnCp_2$

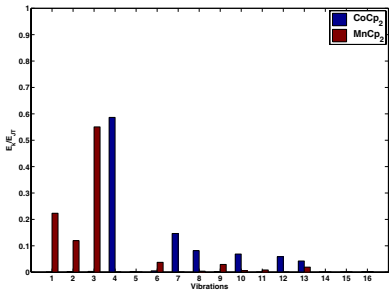

(b) Energetic Contribution of the 16 a_1 normal modes in C_{2v} (LS) to the E_{JT} in blue $CoCp_2$ and in red $MnCp_2$

Figure 6: Analysis of the multimode JT effect in the HS point of cobaltocene and manganocene

metal-ring stretch.

On the first sight it may look surprisingly that these two very similar systems show this significant difference. But if we look into their electronic structure we see that this result is actually expected [23]. Cobaltocene in D_{5h}, is in the electronic ground state E_1'', with a single electron in a double degenerate e_1'' MO. This MO is antibonding between metal d_{xz} (or d_{yz}) and ligand π system. Manganocene is on the other hand in E_2' ground state,

with a single hole in almost non-bonding d_{xy} ($d_{x^2y^2}$). These MOs and most important JT vibrations are depicted on the Fig. 7 and Fig. 8.

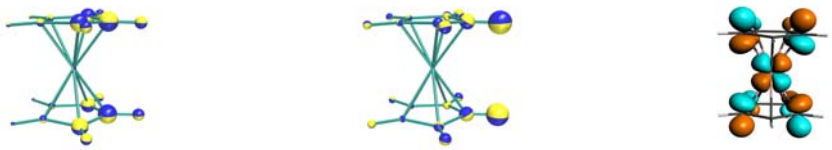

(a) Vib.4 corresponding to e_2', 587 cm^{-1}, out-of-plane ring deformation

(b) Vib.8 corresponding to e_2', 869 cm^{-1}, C−H wagging

(c) Single Occupied Molecular Orbital of $CoCp_2$; $e_1''(d_{xz})$

Figure 7: Rationalisation of the JT Distortion in $CoCp_2$—Vibrational energy distribution representation of Vib.4, (a) and Vib.8, (b) and Single Occupied Molecular Orbital (c)

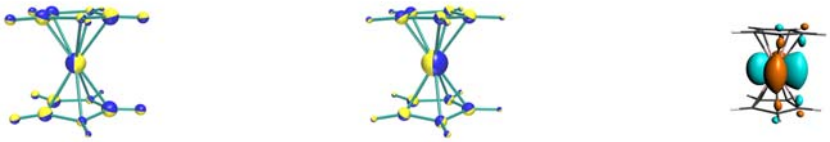

(a) Vib.1 corresponding to e_1', 158 cm^{-1}, skeletal bending

(b) Vib.3 corresponding to e_1', 525 cm^{-1}, ring tilt

(c) Single Occupied Molecular Orbital of $MnCp_2$; $e_2'(d_{xy})$

Figure 8: Rationalisation of the JT Distortion in $MnCp_2$—Vibrational energy distribution representation of Vib.1, (a) and Vib.3, (b) and Single Occupied Molecular Orbital (c)

It is clearly seen that out-of-plane type vibrations of e_2' type in cobaltocene minimize the antibonding interaction between the singly occupied d-orbital and the π-system of the cyclopentadienyl rings. In the case of manganocene e_1' vibrations are enhancing the small bonding interactions between the d-orbital and the π system. This is in agreement with the results of our qualitative analysis [3]. As the distortion of $MnCp_2$ is localized around the metal ion, only skeletal type of vibrations are contributing to the distortion, e.g–bending, tilting and metal-ring stretch. Distortion in $CoCp_2$ is delocalized on the cyclopentadienyl rings, so the distortion modes of the ligands are the most important deformation modes (Fig. 6), e.g. Vib. 7 and Vib. 10.

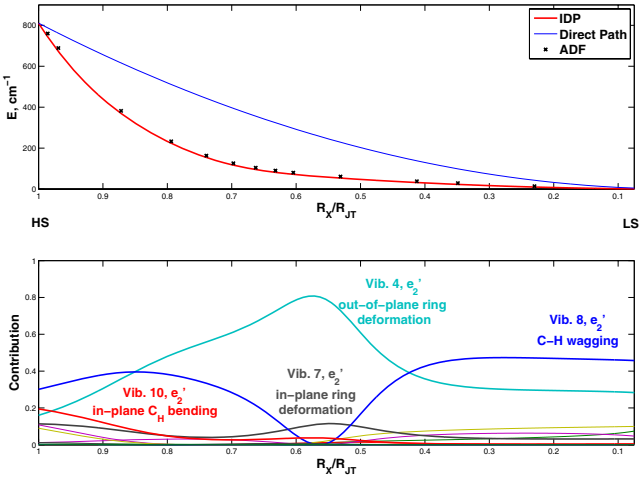

(a) Difference between the Direct Path and IDP (up) and changes of contributions (normalized to 1) of the 16 normal modes to the distortion along IDP (down) for $CoCp_2$

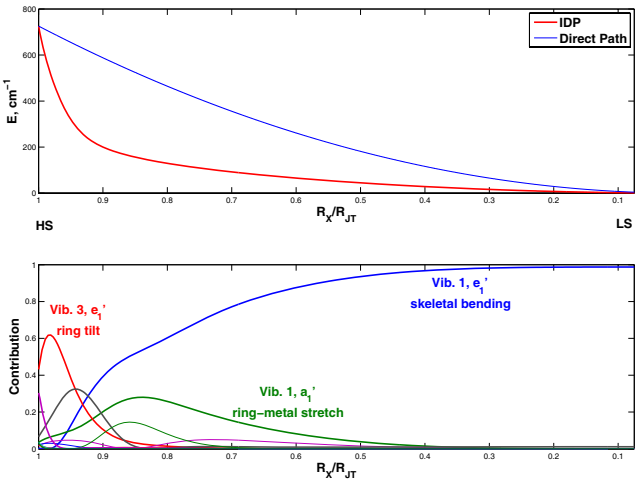

(b) Difference between the Direct Path and IDP (up) and changes of contributions (normalized to 1) of the 16 normal modes to the distortion along IDP (down) for $MnCp_2$

Figure 9: Results of the IDP method for the JT distortion in cobaltocene (a) and manganocene (b)

Further details about the distortion in metallocenes is obtained analysing the IDP from the HS structure to the LS minimum. Figure 9 shows the energy differences between the IDP and the Direct Path for both $CoCp_2$, Fig. 9 (a), and $MnCp_2$, Fig. 9 (b). In both cases the IDP is steeper and the system is strongly stabilized very early along the path. This trend is more distinct in $MnCp_2$. The energies obtained by the IDP method are in excellent agreement with the DFT results, i.e. for cobaltocene $E_{\mathrm{JT}}(\mathrm{IDP}) = 808$ cm^{-1} and for manganocene $E_{\mathrm{JT}}(\mathrm{IDP}) = 725$ cm^{-1}

On the potential energy profiles it is possible to distinguish two distinct regions. In the first part energy is changing faster, thus ca. 80% of the E_{JT} is obtained early along the IDP. In the case of $MnCp_2$ this is achieved already after 10% and in the case of $CoCp_2$ after around 40% of the path. In the second region the change of the energy is small, adiabatic potential energy surface is flat and the molecule just relax towards the global minimum.

The changes of the contributions of the different normal modes to the total force along the IDP are shown on Fig. 9. In the case of $CoCp_2$ out-of-plane ring deformation, Vib. 4, and C-H wagging (the out-of-plane C−H bending), vib. 8, are the most important for the JT distortion, Fig. 9 (a). As the distortion deviates from the HS point contribution of Vib. 8 decreases to zero around 50% of IDP, then it starts to increase again, and the molecule relaxes towards the minimum conformation. For the Vib. 4 which is the most important one, the opposite trend is observed. The contribution of this normal mode increases and becomes dominating in the middle of the path and decreases afterwards again. The JT distortion of $MnCp_2$ starts along the Vib. 3 (tilting), Fig. 9 (b), the harder of the two skeletal vibrations that stabilize the Single Occupied MO, as explained above. All the changes occur in the first region of the IDP, Fig. 9 (b). The importance of softer of two modes, skeletal bending, increases with increasing deviation from the HS point. Vib. 3 (tilting) reaches the equilibrium value after ca. 20% of the path. In further region it is mainly the softer skeletal bending mode, Vib. 1 along which the energy minimum is approached.

This example shows that there is a sophisticated competition between the electronic distortion due to the JT effect, mainly localized on the central metal ion, and the distortion of the ligand conformation in metal complexes, which defines the LS structure. In the case of cobaltocene distortion is mainly localized on the ligands. The symmetry of the electronic ground state in HS point focuses the distortion to the perturbation of the aromaticity of the two rings. In manganocene the distortion is localized around metal,

thus only skeletal type of vibrations are responsible for the distortion and cyclopentadienyl rings remain planar.

4. Conclusions and Perspectives

DFT is today the most common theoretical method in quantum chemistry, and it can be successfully applied for a detailed analysis of the JT effect. This is a challenge due to the superposition of effects produced by many different vibrational modes. In this paper we presented extension of our method for the analysis of the multimode JT effect using concept of the Intrinsic Distortion Path. Inspection of the path of minimal energy from the HS point towards the LS energy minimum gives the detailed information on the vibronic coupling, not possible to get from the experimental data. This enables us to take the first step in answering the questions which we posed in the Introduction of this paper.

Within the harmonic approximation, it is possible to quantify the contributions of different normal modes to the distortion and to the energy stabilisation. In certain cases, only one mode dominates the distortion, but in general this is not the case. Illustration of this can be VCl_4 where the contribution of the angle bending e mode to the distortion is more than 99 % [3]. Under this conditions the classical model is sufficient to discuss the details of the JT distortion. In general the IDP differs from the direct path, defined by the distortion vector between the HS point and the LS minimum. The discrepancy between the two is smaller for the simpler systems, e.g Cu_3. It is obvious that the contributions of the normal modes to the distortion are changing along the IDP. In the beginning the JT active modes that are the basis of the non-totally symmetric irreps in the HS point group are dominating. A simple one-electron description (MOs) can be useful in rationalizing which normal modes are the most adequate for the energy stabilization due to the distortion. If there are several appropriate vibrations, harder ones will be dominant in the first step, while the softer ones take over along the IDP. The contribution of the other modes is expected to become more important for the direction of the relaxation with increasing deviation from the high symmetry geometry. The contribution to the stabilization energy however is minor.

Conceptually simple model presented here gives the direct insight into the one of the essential problems in the physical chemistry–coupling between the electron distribution and the motion of the nuclei. Systematic analysis

of the JT distortions of more molecules with different symmetries should be undertaken in order to develop a feeling for the qualitative estimation of this interaction. Further extensions of this procedure should be inclusion of the anharmonicity as well as the investigation of the vibronic coupling of the ground and excited states (Pseudo Jahn-Teller effect).

Final remark should be made concerning the localisation/delocalisation of the JT distortion in metal complexes. The electronic distortion due to the JT effect is mainly localized on the central metal ion, but as seen on the example of cobaltocene it can be delocalized over the ligands. In other words the JT effect induces conformational changes of the ligands which counterbalance the JT distortion. The importance of this influence is well documented in the book by Bersuker [36]. This is expected in various JT active chelate complexes. This can be of great significance in understanding the reactivity changes of the ligands in the biologically important molecules, e.g. Cu^{2+} proteins, or spin-crossover compounds, mixed valence compounds, photochemical reactions etc.

Acknowledgements

This work was supported by the Swiss National Science Foundation and the Serbian Ministry of Science (Grant No. 142017G). MGP acknowledges Serbian Ministry of Science for the postdoctoral fellowhsip during which time part of this work was done.

References

[1] H A. Jahn, E. Teller, Stability of Polyatomic Molecules in Degenerate Electronic States. I. Orbital Degeneracy, Proc. R. Soc. London, Ser A 161 (1937) 220–235.

[2] I. B. Bersuker, The Jahn-Teller Effect, Cambridge University Press, 2006.

[3] M. Zlatar, C.-W. Schläpfer, C. Daul, in H. Köppel, D. R. Yarkoni, H. Barentzen (Eds.), The Jahn-Teller-Effect Fundamentals and Implications for Physics and Chemistry, Series: Springer Series in Chemical Physics, Vol. 97 (2009) 131–165.

[4] R. F. W. Bader, An Interpretation of Potential Interaction Constants in Terms of Low-lying Excited States, Mol. Phys. 3 (1960) 137–151.

[5] R. F. W. Bader, Vibrationally Induced Perturbations in Molecular Electron Distributions, Can. J. Chem. 40 (1962) 1164–1175.

[6] R. F. W Bader , A. D. Bandrauk, Relaxation of the Molecular Charge Distribution and the Vibrational Force Constant, J. Chem. Phys. 49 (1968) 1666–1675.

[7] R. G. Pearson, A symmetry Rule for Predicting Molecular Structures, J. Am. Chem. Soc. 91 (1969) 4947–4955.

[8] R. G. Pearson, Symmetry Rules for Chemical Reactions, A Willey-Interscience Publication, 1976.

[9] K. Fukui, Formulation of the Reaction Coordinate, J. Phys. Chem. 74 (1970) 4161–4163.

[10] K. Fukui, The path of Chemical Reactions–the IRC Approach, Acc. Chem. Res. 14 (1981) 363–368.

[11] Y. Liu, I. B. Bersuker, W. Zou, J. E. Boggs, Combined Jahn-Teller and Pseudo-Jahn–Teller Effect in the CO_3 Molecule: A Seven-State Six-Mode Problem, J. Chem. Theory Comput. 5 (2009) 2679–2686.

[12] Adf2007.01. SCM, Theoretical Chemistry, Vrije Universiteit Amsterdam, The Netherlands, http://www.scm.com (2007)

[13] C. F. Guerra, J. G. Snijders, G. te Velde, E. J. Baerends, Towards an Order-n DFT Method, Theor. Chem. Acc. 99 (1998) 391–403.

[14] G. te Velde , F. M. Bickelhaupt, S. J. A. van Gisbergen, C. F. Guerra, E. J. Baerends, J. G. Snijders, T. Ziegler, Chemistry with ADF, J. Comput. Chem. 22 (2001) 931–967.

[15] S. Vosko, L. Wilk, M. Nusair, Accurate Spin-Dependent Electron Liquid Correlation Energies for Local Spin Density Calculations: a Critical Analysis, Can. J. Phys. 58 (1980) 1200.

[16] A. Bérces, R. M. Dickson, L. Fan, H. Jacobsen, D. Swerhone, T. Ziegler An Implementation of the Coupled Perturbed Kohn–Sham Equations: Perturbation Due to Nuclear Displacements, Comput. Phys. Commun. 100 (1997) 247–262.

[17] H. Jacobsen, A. Bérces, D. Swerhone, T. Ziegler, Analytic Second Derivatives of Molecular Energies: a Density Functional Implementation. Comput. Phys. Commun. 100 (1997) 263–276.

[18] M. Fedorovsky, Pyvib2, A Program for Analyzing Vibrational Motion and Vibrational Spectra. http://pyvib2.sourceforge.net (2007).

[19] R. Bruyndockx, C. Daul, P. T. Manoharan, E. Deiss, A Nonempirical Approach to Ground-State Jahn-Teller Distortion: Case Study of VCl_4. Inorg. Chem. 36 (1997) 4251–4256.

[20] F. A. Blankenship, R. L. Belford, VCl_4 Vapor Spectrum and Jahn-Teller Splitting, J. Chem. Phys. 36 (1962) 633–639.

[21] Y. Morino, H. Uehara, Vibronic Interactions in Vanadium Tetrachloride by Gas Electron Diffraction, J. Chem. Phys. 45 (1966) 4543–4550.

[22] R. B. Johannesen, G. A. Candela, T. Tsang, Jahn-Teller Distortion: Magnetic Studies of Vanadium Tetrachloride, J. Chem. Phys. 48 (1968) 5544–5549.

[23] J. H. Ammeter, L. Zoller, J. Bachmann, P. Baltzer, E. Gamp, R. Bucher, E. Deiss, The Influence of Molecular Host Lattices on Electronic Properties of Orbitally (near-) degenerate Transition Metal Complexes, Helv. Chim. Acta. 64 (1981) 1063–1082.

[24] B. E. Applegate, A. J. Bezant, T. A. Miller, The Jahn-Teller and Related Effects in the Cyclopentadienyl Radical. II. Vibrational Analysis of the $\tilde{A}\ ^2A_2''$–$\tilde{X}\ ^2E_1''$ Electronic Transition, J. Chem. Phys. 114 (2001) 4869–4882.

[25] M. Zlatar, C.-W. Schläpfer, E. P. Fowe, C. Daul, Density Functional Theory Study of the Jahn-Teller Effect in Cobaltocene, Pure. Appl. Chem. 81 (2009) 1397–1411.

[26] R. Bucher, ESR-Untersuchungen an Jahn-Teller-Aktiven Sandwitchkomplexen, PhD thesis, ETH Zürich, 1977.

[27] J. H. Ammeter, N. Oswald, R. Bucher, Dynamische Jahn-Teller Verzerrungen und chemische Bindungsverhältnisse in orbitalentarteten Sandwitchkomplexen, Helv. Chim. Acta, 58 (1975) 671–682.

[28] T. K. Kundu, R. Bruyndonckx, C. Daul, P. T. Manoharan, A Density Functional Approach to the Jahn-Teller Effect of $[Cu(en)_3]^{2+}$ as a Model for a Macrobicyclic Cage Complex of Copper(II), Inorg. Chem. 38 (1999) 3931–3934.

[29] E. Gamp, ESR-Untersuchungen über den Jahn-Teller-Effekt in oktaedrischen Kupfer (II)-Komplexen mit trigonalen dreizähnigen Liganden, PhD Thesis, ETH Zürich, 1980.

[30] A. Ceulemans, L. G. Venquickenborne, The Epikernel Principle, Structure and Bonding, 71 (1989) 125–159.

[31] A. Ceulemans, D. Beyens, L. G. Venquickenborne, Symmetry Aspects of Jahn-Teller Activity: Structure and Reactivity, J. Am. Chem. Soc. 106 (1984) 5824–5837.

[32] P. Garcia-Fernandez, I. B. Bersuker, J. A. Aramburu, M. T. Barriuso, M. Moreno, Origin of Warping in the $E \otimes e$ Jahn-Teller Problem: Quadratic Vibronic Coupling Versus Anharmonicity and Application to NaCl:Rh^{2+} and Triangular Molecules, Phys. Rev. B. 71 (2005) 184117–1–10.

[33] W. Hug, M. Fedorovsky, Characterizing Vibrational Motion Beyond Internal Coordinates, Theor. Chem. Acc. 119 (2008) 113–131.

[34] Z. F. Xu, Y Xie, W. L. Feng, H. F. Schaefer III, Systematic Investigation of Electronic Structures for the First Transition Metal Series Metallocenes $M(C_5H_5)_2$ (M= V, Cr, Mn, Fe, Co and Ni), J. Phys. Chem. A 107 (1997) 2176–2729.

[35] M. Swart, Metal-ligand Bonding in Metallocenes: Differentiation Between Spin State, Electrostatic and Covalent Bonding, Inorg. Chim. Acta. 360 (2007) 179–189.

[36] I. B. Bersuker, Electronic Structure and Properties of Transition Metal Compounds, John Wiley & Sons, INC. 1996.

Supplementary Material

Table S1: Analysis of the JT multimode problem in cobaltocene and manganocene by LS totally symmetric normal modes in harmonic approximation. Frequencies of normal modes are in cm^{-1} as obtained from ADF [12, 14, 13] calculations; contribution of the normal mode $\vec{Q}_k$ to the distortion is given by c_k in %; E_k energy contribution of $\vec{Q}_k$ to the E_{JT} in cm^{-1}

			$CoCp_2$			$MnCp_2$		
$\vec{Q}_k$	Assignment	HS-irrep	$\tilde{\nu}_k$ in C_{2v}	c_k	E_k	$\tilde{\nu}_k$ in C_{2v}	c_k	E_k
1	skeletal bending	e_1'	153	0.03	0.02	160	78.48	162.10
2	ring–metal stretch	a_1'	292	0.80	1.95	305	9.73	86.71
3	ring tilt	e_1'	405	0.25	0.03	502	8.70	399.61
4	out-of-plane ring deformation	e_2'	587	64.95	475.49	652	0.01	0.33
5	C−H wagging	a_1'	762	0.58	2.11	796	0.00	0.01
6	C−H wagging	e_1'	825	0.82	4.12	818	1.76	27.06
7	in-plane ring distortion	e_2'	830	10.44	118.86	838	0.00	0.00
8	C−H wagging	e_2'	869	11.66	66.22	898	0.11	2.81
9	C−H bending	e_1'	976	0.19	1.44	996	0.83	21.25
10	in-plane C−H bending	e_2'	1031	8.09	55.77	1031	0.18	4.12
11	ring breathing mode (C−C	a_1'	1126	0.00	0.00	1132	0.04	6.11
12	C−C stretch	e_2'	1367	1.18	47.86	1378	0.00	0.04
13	C−C stretch	e_1'	1397	0.93	34.15	1422	0.11	13.86
14	C−H stretch	e_2'	3136	0.01	0.46	3127	0.00	0.10
15	C−H stretch	e_1'	3148	0.00	0.13	3139	0.00	0.37
16	C−H stretch	a_1'	3166	0.00	0.00	3151	0.00	1.20